F

Internal Report
DESY D3 - 95
December 1999

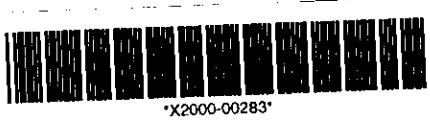

Calculation of hadron yields around thick targets and doses behind concrete shielding of high energy electron accelerators

H. Dinter, A. Leuschner, K. Tesch
Deutsches Elektronen-Synchrotron DESY, Hamburg
and
D. Dworak, J. Łoskiewicz
Institute of Nuclear Physics, Kraków

"Die Verantwortung für den Inhalt dieses
Internen Berichtes liegt ausschließlich beim Verfasser"

Internal Report
DESY D3 - 95
December 1999

Calculation of hadron yields around thick targets and doses behind concrete shielding of high energy electron accelerators

H. Dinter, A. Leuschner, K. Tesch
Deutsches Elektronen-Synchrotron DESY
Notkestr.85, D-22603 Hamburg, Germany
and
D. Dworak, J. Łoskiewicz
Institute of Nuclear Physics
Ul. Radzikowskiego 152, 31-342 Kraków, Poland

To be published in Nuclear Instruments and Methods

Abstract

The field of neutrons, protons, and pions produced by high energy electrons hitting thick targets is studied by means of the FLUKA Monte-Carlo code. Particle spectra and dependences of fluences on primary energy (1 GeV to 250 GeV), on angle (20^{o} to 150^{o}) and on target mass number are given, together with the total number of low energy neutrons and of high energy neutrons per electron. The attenuation of the total hadron dose equivalent in concrete and dose ratios of the main components are calculated. All results are parametrized and expressed by simple formulae. Also studied is the hadron field behind copper and lead absorbers (beam shutters) in beam direction, its composition and its dependence on primary energy (1 GeV to 50 GeV), on distance, and on absorber type. Again the total hadron dose equivalent can be expressed by a simple equation. The dose attenuation by an additional concrete shield behind an absorber is also examined.

1. Introduction

Monte Carlo codes have proved to be the most important tools in calculating particle production and shielding. With modern computers significant results can be gained even in complicated geometries and moderately thick shieldings up to the highest primary energies. However, the effort in using comprehensive code systems is considerable and computing times are always high. Therefore it is desirable to have simple formulae at hand for cases in which the actual situation can be approximated by a simplified geometry. In many cases this procedure is sufficient for existing or future accelerator shielding design, and more accurate calculations may be unnessesary in view of the fact that very often the accuracy of calculated doses does not depend on any calculational method but on the insufficient knowledge of the number of absorbed primary particles. Such formulae can be derived from extensive Monte Carlo calculations.

Formulae of this kind are available for calculation of hadron doses at proton accelerators, see [1] for lateral shielding and [2] for longitudinal shielding, and papers quoted there. Other recent shielding calculations are given in [3] and [4]. Photon doses behind concrete shielding at proton accelerators are calculated in [5]. Numerous publications are addressed to neutron shielding, recent papers are [6, 7] .

For electron accelerators the lateral shielding of the electromagnetic component ($e^{\pm}$, γ) is studied in [8]. This dose depends strongly on target geometry, so several target configurations and materials were examined and the results condensed to formulae covering the angular range 5^{O} to 140^{O}. Electron-photon doses behind absorbers (in beam direction) are calculated in [9].

Missing are simple equations for calculating hadron doses around shielded targets at electron accelerators. Since a few years, the hadron production by photons has been incorporated in the well-known FLUKA Monte Carlo code [10]. (Direct electro-hadron production can be neglected in thick targets, see [11].) We used this possibility to calculate dose equivalents of neutrons, protons and pions (and also of electrons and photons) around thick targets of different materials and their attenuation in concrete in the angular region 20^{O} to 150^{O} for primary electron energies E_o between 1 GeV and 250 GeV and also at $\theta = 0^{O}$ (beam stop geometry) for E_o= 1 GeV to 50 GeV. The results were parametrized to receive simple equations for calculating the total dose equivalent. Detailed results are compiled in an internal report [12].

2. Hadron doses in the angular intervall 20^{O} to 150^{O}

2.1. Target geometry

When an electron beam hits a target, the produced electron-photon doses depend strongly on its shape, see e.g. [8], where several target geometries are studied. When dealing with hadron doses the target should be rather thick so that the maximum number of hadrons is produced whereas the internal absorption of hadrons is still low. This means a target which is just large enough for the electromagnetic cascade to be fully developed.

We used targets of cylindrical shape, the length is chosen so that 10% of the radially integrated energy is lost longitudinally, and the radius is chosen so that 10% of the longitudinally integrated energy is lost radially. The resulting dimensions for all primary energies are shown in tab.1, the used cascade data are taken from [13]. These cylinders are hit on axis by a one-dimensional electron beam.

Material	Radius	Length [cm] for a primary energy of					
	[cm]	1 GeV	3 GeV	10 GeV	30 GeV	100 GeV	250 GeV
Al	12	70	85	100	112	125	137
Cu	4	14	17	20	22	24	26
Nb	5	12	15	16	19	20	22
Pb	2	7	7	7	8	8	8

Table 1: Dimensions of targets used in the calculations.

The calculated doses around these thick targets can be representative for cases when a beam hits an obstacle, e.g. a collimator or any other machine component because of beam missteering. They may be the basis for discussing worst-case scenarios.

2.2. Radiation field around targets

Before considering the attenuation of hadron doses in concrete we studied the radiation field around the targets in the total angular range for all 4 target materials and for all 6 primary energies (see tab.1). The FLUKA code was used in fully analogue manner to calculate fluences of neutrons, protons and pions. The boundary-crossing estimator was used. Low-energy cuts were set at 1 MeV for electrons, positrons, photons, protons and pions, and neutrons were calculated down to thermal energy. Some of the results are presented in the following.

First we studied the shape of the fluence spectra of neutrons, protons and pions and their dependence on primary energy E_o and on target material. Two examples are shown in figs.1 and 2. At large angles (80^O to 100^O) the typical contribution of particles from the intranuclear cascade (around 100 MeV) and the low energy neutrons show up. It turns out that the shapes of all spectra at large angles (80^O to 100^O) are independent of E_o and material in the considered primary energy range. This is also true at 20^O to 30^O if $E_o \geq 30$ GeV, for $E_o \leq 10$ GeV the high energy tail decreases as expected. It is interesting to study separately the neutron spectra produced by the 4 interaction mechanisms incorporated in the FLUKA code: giant-resonance interaction, quasi-deuteron disintegration, production of the Δ-resonance, interaction with photon energies above 0.7 GeV. Fig.3 gives an example.

The dependence of the fluences on the primary energy is a simple power law $\Phi \sim E_o^a$; the exponent a is nearly the same for the angle-integrated fluences and for all fluences in a specified angular interval. For neutrons below 150 MeV a mean $\bar{a}$ is 1.0 ± 0.06, for neutrons of higher energies and for protons and pions $\bar{a}$ is 1.1 ± 0.06. The values are higher than for incoming protons where $\bar{a}$ is 0.7 due to partitioning of the primary energy between the hadronic and the electromagnetic cascades [1].

Tab.2 demonstrates the dependence of hadron production on mass number A of the target for 4 hadron components. The expected increase of low energy ($E_n < 20$ MeV) neutron production with increasing A (see e.g. ref.[14]) is somewhat reduced due to absorption in our thick targets. The production of high energy neutrons and charged particles decreases with increasing A as a result of reduced radiation lengths within the electromagnetic cascade and enhanced intranuclear interactions at large A. The relative A- dependence agrees with measurements of neutrons above 25 MeV performed at $E_o = 6.3$ GeV many years ago [15]. The variation in production numbers is small for $A > 90$, therefore we dropped shielding calculations for a lead target in section 2.3.

Target		Neutrons		Protons	Charged Pions
	A	$E_n < 20$ MeV	$E_n > 20$ MeV		
Al	27	2.2	0.28	0.020	0.035
Cu	64	4.2	0.19	0.011	0.018
Nb	93	8.2	0.16	0.008	0.013
Pb	207	8.2	0.14	0.012	0.012

Table 2: Calculated numbers of particles produced by one 30-GeV electron in 4 targets with dimensions shown in tab.1

The calculation of secondary particles around the targets gives the opportunity to compare the total number of produced neutrons with other calculations and with measurements, see tab.3 where the numbers of neutrons below and above 20 MeV per one 1-GeV primary electron are displayed; for high energy neutrons the calculated data are derived from 10-GeV results and the experimental data from 6.3-GeV results, both scaled down to 1 GeV for comparison. The low energy data are in only moderate agreement. The experimental results seem to be higher than the calculated ones except in the recent work of Degtyarenko et al. [16] who used a new nuclear fragmentation model. A decision cannot be made, new and better experiments are necessary. For comparison with the high energy results we found only our rather old data [15], they were somewhat reduced because of more recent information on the cross-section of the then used activation reaction. Again the calculated values are smaller than the measured ones, about by a factor of 2.

Target mat.	$E_n < 20$ MeV Calculations: This work	Swanson [17]	Mao et al. [11]	Degtyarenko et al. [16]	Measurements from compilation [13]		$E_n > 20$ MeV: This work	Bathow et al. [15]
Al	0.074	0.10	0.068		Bathow	0.18	0.0088	0.02
Cu	0.14	0.19	0.16	≈ 0.28	Bathow	0.35	0.0063	0.013
					DeStabler	0.19		
					Stevenson	0.33-0.45		
Pb	0.28	0.34	0.30		Bathow	0.41	0.0045	0.009

Table 3: Number of neutrons produced per 1-GeV primary electron in thick targets.

Finally, we mention briefly the angular distribution of hadrons around a target. The relative angular distribution is nearly independent of the primary energy since the exponent a in the expression E_o^a was found to be nearly the same for all angular intervals (see above). Therefore the distributions are displayed in fig.4 only for $E_o = 30$ GeV and a copper target. The low energy neutrons show a peak around 90^O which is unexpected since giant-resonance neutrons are essentially isotropic, and neutrons and protons show a flat distribution at small angles, also against expectation. The reason is internal attenuation in our thick cylindrical target which disturbs the original isotropic distributions. As a check we repeated the calculations with a small target 5 cm × 3 cm ø which gave a flat distribution for low energy neutrons and a distribution peaked at 0^O for higher energies. However, in this work we deal with thick targets, so we have to accept the distributions of fig.4.

2.3. Doses behind concrete shielding

In order to calculate dose equivalents behind concrete shields and the associated dose equivalent attenuation coefficients, the targets described in tab.1 were surrounded by a spherical concrete shell with a thickness of 360 cm and positioned at a distance r between 500 cm and 860 cm from the midpoint of the target. We could reduce the available parameter considerably according to the results of the preceding section. Only two primary energies were selected: E_o=30 GeV to receive results for $E_o \geq 10$ GeV, and E_o=3 GeV for results with $E_o \leq 10$ GeV. The change in spectra from the niobium target to the lead target is small, so we received the A-dependence for $A < 100$ from Al, Cu and Nb targets and took the niobium results as being representative for the $A > 100$ region. Four angular intervals $\Delta\theta$ were selected: 20^O to 30^O, 50^O to 60^O, 80^O to 100^O, 140^O to 160^O. One-way fluences of neutrons, protons and pions were calculated by the FLUKA code, the hadron production cross-sections were artifically increased by a factor of 50. Dose equivalents were calculated from the fluences by multiplication with fluence-to-dose conversion factors, we used the same factors as in [1] to receive the maximum dose in a 30-cm phantom. In addition to hadrons, also photon fluences with energies above 1 MeV and doses were calculated in all cases. Examples of the neutron spectra are displayed in fig.5 in a concrete depth $d = 60$ cm to show the shaping effect of the concrete.

Next we will discuss the attenuation of the total hadron dose and its components. An example of hadron dose equivalent attenuation is shown in fig.6 for the 4 ranges of angle θ. A steep and a flat exponential decrease are observed. In the fig.7 the hadron dose is split into 4 components: neutrons above 20 MeV, neutrons below 20 MeV, protons and charged pions. One can see that at 90^O the steeply decreasing component usually attributed to low-energy neutrons is due to the charged particles and to neutrons below 20 MeV. Incidentially the combined effect of both gives nearly the same dose equivalent attenuation coefficient $\lambda_1 = 28$ g/cm^2 for all examined E_o, A, and for angles θ with a pronounced steeply decreasing component (see below). This value is lower than 48 g/cm^2 recommended for low-energy neutrons [13], lower than 42 g/cm^2 measured with isotopic neutron sources [18], and somewhat lower than 33 g/cm^2 from other recent calculations in the lower GeV range [16]. The slowly decreasing hadron dose component is produced by high and low-energy neutrons being in radiation equilibrium behind concrete thickness larger than about 80 cm and by charged particles (at large angles by protons also in equilibrium with neutrons). The ratio of these components is of interest since in many cases only the dose of neutrons below 20 MeV is measured. Mean values are calculated for 3 targets, E_o=3 GeV and 30 GeV, $\theta = 25^O$ and 90^O, $d > 80$ cm concrete. The dose equivalent ratio of neutrons above 20 MeV to dose of low-energy neutrons is 1.9±0.2, high energy neutrons are the main neutron dose equivalent component

in all considered cases. The dose ratio charged particles to low-energy neutrons decreases at small angles from 2.6 to 1.3 with increasing concrete thickness for E_o=30 GeV, and from 1.4 to 0.3 for E_o = 3 GeV. At 90^O it is 0.4 and independent of primary energy and shielding thickness. The charged particles are only protons at 90^O and $d > 80$ cm concrete, at 25^O pions contribute up to 200 cm concrete.

In fig.7 the electron-photon dose H_γ is also shown. It is the dominating component behind thin concrete shielding. One should note, however, that H_γ depends strongly on target shape, so H_γ is better calculated from our earlier paper [8]. These earlier results agree with results of this work within a factor of 2 for roughly similar geometries. However, the hadrons deteriorate the purely exponential decrease of H_γ at larger thicknesses, the beginning of an equilibrium between hadron dose and photon dose is indicated in fig.7 at a level of $H_\gamma/H_h \approx 0.02$.

The 90^O curve of fig.7 for high energy neutrons and larger concrete thickness can be compared with our earlier paper [19] which is a compilation of earlier calculations and measurements of high energy neutron doses. The attenuation coefficient is nearly the same, the absolut values agree within a factor of 2. Another comparison can be made with the first hadron dose calculation behind thick shielding at electron accelerators [20], here only star densities were calculated and a general ratio star density to dose assumed. At 25^O and 55^O a fair agreement with fig.7 is received, at 90^O the values disagree because of a smaller attenuation coefficient in [20].

All total hadron dose equivalents per primary electron behind concrete shielding calculated up to $d = 360$ cm, for $E_o = 3$ GeV and 30 GeV and for Al, Cu, and Nb targets can be expressed by

$$H_h \cdot r^2 = a_1 \, e^{-d/\lambda_1} + a_2 \, e^{-d/\lambda_2} \tag{1}$$

d and r are concrete thickness and distance. The parameters $\lambda_{1,2}$ and $a_{1,2}$ were parametrized with the following results. λ_1 could be fixed for all cases (see above):

$$\lambda_1 = 28 \text{ g/cm}^2 \tag{2}$$

λ_2 depends weakly on angle θ but not on E_o or mass number A.

$$\lambda_2 = (91 + 52 \, e^{-\theta/33^o}) \text{ g/cm}^2 \tag{3}$$

The dependence of a_1 and a_2 on E_o, A and θ was discussed qualitatively in section 2.2.

$$a_1 = 0.29 \, A^{2/3} \, \frac{E_o}{1\text{GeV}} \, (0.33 + 0.67 \sin(\theta)) \text{ pSv cm}^2 \tag{4}$$

$$a_2 = 81 \, A^{-4/5} \left(\frac{E_o}{1\text{GeV}}\right)^{1.1} (0.04 + 0.96 \, e^{-\theta/24^o}) \text{ pSv cm}^2 \tag{5}$$

The hadron doses calculated from eqs.(1)-(5) agree well with the original FLUKA results up to a primary energy of 250 GeV. The equations are valid for $\theta > 20^O$ and for $A < 100$, for $A > 100$ the results with $A = 100$ are a sufficient approximation.

If only neutron dose equivalents are of concern the best fits for a_1 and a_2 are

$$a_1 = 0.24\, A^{2/3}\, \frac{E_o}{1\mathrm{GeV}}\, (0.33 + 0.67 \sin(\theta))\ \mathrm{pSv\ cm^2} \tag{6}$$

$$a_2 = 23\, A^{-2/3}\, \left(\frac{E_o}{1\mathrm{GeV}}\right)^{1.1}\, (0.07 + 0.93\, \mathrm{e}^{-\theta/31^o})\ \mathrm{pSv\ cm^2} \tag{7}$$

Neutron doses calculated with eqs.(1)-(3), (6), and (7) can be compared with the most recent calculation of neutron doses for the energy range $E_o = 0.2$ to 8 GeV [16]. The authors use the same fit as in equ.(1). We compared both results for E_o=3 GeV. λ_1, λ_2 and the θ-dependence of λ_2 is only slightly different from our results. The values of a_1 and a_2 of ref.[16], however, are a factor 2.5 to 3 higher, this was already discussed in section 2.2 and tab.3.

It is not easy to estimate the reliability of results received by eqs.(1)-(7) (and by the equations of the next section) quantitatively. Main reasons are the dramatic lack of published dose measurements behind shielding at high primary energies, the contribution of high energy neutrons and (in several cases) of charged particles, the use of selected fluence-to-dose conversion factors in calculating dose equivalents. Guided by comparison with other calculations and by the considerations in section 2.2 we estimate an uncertainty of a factor of two in both directions.

Finally we compare our λ_2 values with the corresponding values for primary protons calculated in [1], see tab.4. For primary electrons the θ-dependence is weaker and the λ_2 are smaller at all angles. The reason is the difference in the high-energy tail of the neutron dose spectra. They are shown in fig.8 for 30-GeV protons or electrons on the copper target (see tab.1) at angles 25^O and 90^O; to facilitate the comparison both dose spectra are normalized to unity.

θ [degree]	λ [g/cm^2] primary electrons equ.(3)	primary protons ref.[1]
20-30	115	150
30-40	108	139
40-50	103	137
50-60	101	127
60-70	99	123
70-80	96	113
80-100	94	110
100-120	94	103
120-140	92	117
140-160	92	113

Table 4: Attenuation coefficients of hadron dose equivalents produced by 30-GeV electrons or 30-GeV protons hitting a copper target.

3. Hadron doses behind a beam absorber

The formulae derived in section 2.3 must not be extrapolated to 0^O. But doses just behind an absorber (beamstop, beamshutter) are also of interest at electron accelerators. A simple equation

for calculating electron-photon doses behind absorbers in beam direction is already available for E_o = 0.15 to 50 GeV [9]. Here we add calculations of total hadron doses for 1 GeV to 50 GeV and in addition their attenuation in concrete. (For electron accelerators with energies much higher than 50 GeV a beamshutter geometry seems to be unprobable.)

Selected absorbers are 20, 30, 40, and 50 cm copper, 40 cm lead and a sandwich 20 cm copper plus 20 cm lead. The calculations were performed for E_o=1, 3, 10 and 50 GeV again with the FLUKA code; leading-particle biasing was applied and the hadron production cross-sections were artifically increased by a factor of 50. In [8] a small volume 2 cm ø × 3 cm was the scoring element in which the dose was calculated. Produced hadrons are not so sharply peaked in forward direction as the electromagnetic cascade, so we could choose a disc of 10 cm ø as the scoring surface and a boundary-crossing estimator. The distance r behind an absorber is defined with the point zero at the front face. Only distances $r \geq 100$ cm are considered since smaller distances are of minor practical interest, and doses near the rear face of an absorber would result in unrealistic high values when calculated with a boundary-crossing estimator.

The composition of the hadron field behind the absorbers will be described by a few examples. Fig.9 shows spectra of neutrons, protons and negative pions at r = 100 cm behind a 50 cm copper absorber for E_o=10 GeV and 50 GeV, they are of course much harder than at lateral angles. The composition changes for larger distances because of the different angular distributions. Again we note the dose ratios of high-energy neutrons or charged particles to low-energy neutron dose. Low-energy neutrons (below 20 MeV) are the main neutron dose component. The ratio high-energy neutron dose to low-energy neutron dose increases steadily from 0.1 to 1.3 with increasing length of the copper absorbers and with increasing primary energy; behind the lead it is about 0.2 to 0.3 for all E_o. For E_o=10 GeV and 50 GeV charged particles give the largest contribution to the hadron dose. Details can be taken from tab.5. In cases of dominating charged particle doses the dose contributions of protons, positive pions and negative pions are roughly 1 : 2.5 : 5.

Absorber	$H(E_n < 20$ MeV) : $H(E_n > 20$ MeV) : H(charged)			
	1 GeV	3 GeV	10 GeV	50 GeV
Cu 20cm	1 : 0.12 : 0.05	1 : 0.16 : 0.32	1 : 0.17 : 0.61	1 : 0.19 : 1.4
Cu 30cm			1 : 0.30 : 0.91	
Cu 40cm	1 : 0.57 : 0.34	1 : 0.61 : 1.0	1 : 0.66 : 2.2	1 : 0.58 : 3.7
Cu 50cm	1 : 1.4 : 0.7	1 : 1.2 : 1.0	1 : 1.1 : 3.6	1 : 1.3 : 8.1
Pb 40cm	1 : 0.17 :	1 : 0.18 : 0.18	1 : 0.22 : 0.83	1 : 0.28 : 1.7
Cu 20cm + Pb 20cm	1 : 0.26 : 0.08	1 : 0.28 : 0.23	1 : 0.32 : 1.1	1 : 0.31 : 1.9

Table 5: Dose equivalent ratios of neutrons below 20 MeV, neutrons above 20 MeV, and charged particles (protons and pions) for 4 primary energies at r = 100 cm.

Next we discuss the dependence of total hadron dose on the absorber type, distance r and E_o. The r-dependence can be complicated since a point of hadron production within the absorber is not fixed, the angular distributions of hadron components are different, and our 10 cm ø scoring area remains the same at all distances. A fit with $H \sim r^{-b}$ gives a mean value b = 2.24 for all E_o and all absorber types, but b = 2 gives also a reasonable fit, so we take this value. The E_o-dependence is described again as a power law. The exponent depends weakly on absorber typ,

but a mean value is sufficiently accurate. We received

$$H_h \cdot r^2 = a \left(\frac{E_o}{1\,\mathrm{GeV}}\right)^{1.75} \tag{8}$$

per primary electron, $r \geq 100$ cm, and a in tab.6. The mean ratio of values from equ.(8) to original

Absorber	a [pSv cm^2]
Cu 20cm	1.2
Cu 30cm	0.35
Cu 40cm	0.18
Cu 50cm	0.061
Pb 40cm	0.095
Cu 20cm + Pb 20cm	0.25

Table 6: Constants a for equ.(8)

FLUKA results is 1.1 ± 0.7. The largest deviations are for 20 cm copper, but here hadron doses are negligible anyway (see below). If a somewhat cruder approximation is tolerable the data can be further simplified by taking the material thickness D into account which gives for all the selected absorbers

$$H_h \cdot r^2 = 5.2\ \mathrm{e}^{-D/(110\,\mathrm{g/cm^2})} \left(\frac{E_o}{1\,\mathrm{GeV}}\right)^{1.75} \mathrm{pSv\ cm^2} \tag{9}$$

per primary electron, $D > 150\,\mathrm{g/cm^2}$, $r \geq 100$ cm. The mean ratio from equ.(9) to original FLUKA data is now 1.3 ± 0.9. Equ.(9) can be used for absorbers different from our examples.

In many cases the hadron dose is not an important dose behind absorbers, the main component is the electron-photon dose H_γ from the electromagnetic cascade which can also be calculated by a simple equation [9]. It turns out that behind 20 cm and 30 cm copper hadron doses are negligible compared with photon doses, behind 40 cm copper H_h/H_γ is about 0.03, and behind 50 cm it increases from 0.15 to 0.3 with E_o increasing from 1 GeV to 50 GeV. The opposite is true behind our two lead absorbers, here H_γ is negligible and the hadron dose is the only relevant dose component.

Another dose component which may be considered behind beam absorbers is the dose H_μ from muons produced by pair production. In calculating muon doses only coherent production from a nucleus without form factors is to be considered as we deal with small angles and primary energies below 50 GeV. (An overview on relevant production processes can be found in [21].) The resulting muon doses are small compared with the hadron doses at all energies, H_μ/H_h being about 0.01 behind 20 cm copper and 0.1 behind the thicker absorber with 50 cm copper or 40 cm lead. Muons from pion decay are negligible since the flight path for decay is small.

Sometimes a concrete shielding is installed additionally in beam direction behind a copper or lead beamstop. Therefore a concrete cylinder (100 cm ø × 400 cm) was positioned behind an absorber at $r = 100$ cm to 500 cm and the attenuation of hadron doses in the concrete calculated. It turned out that it is not possible to express the results by means of simple equations, instead we give only some general conclusions. No equilibrium between high and low-energy neutrons

is reached in concrete behind absorbers like 20 cm copper or 40 cm lead; the total hadron dose attenuation coefficient rises from 80 g/cm^2 to 140 g/cm^2 with E_o rising from 1 GeV to 50 GeV. In concrete behind 50 cm copper the field is roughly in equilibrium because of the lower fluence of low-energy neutrons reduced in the copper absorber; the attenuation coefficient is about 140 g/cm^2. When starting a calculation of hadron dose behind the concrete with a value from eqs.(8) or (9) and with the mentioned attenuation coefficient one has to take into account a dose buildup in the first 20 cm of concrete, the factor is about 2 for $E_o = 10$ GeV and 4 with $E_o = 50$ GeV. The main dose component in concrete are neutrons for $E_o = 1$ GeV and charged particles (mainly negative pions) for $E_o = 10$ GeV or 50 GeV.

Acknowledgements

All Monte-Carlo calculations were performed at ACK CYFRONET AGH, Kraków, according to grant no. KBN/SPP/IFJ/065/1998 and KBN/S2000/IFJ/065/1998.

References

[1] H.Dinter, K.Tesch, and D.Dworak. *Nucl.Instr.Meth.*, A384:539, 1997.

[2] K.Shin, H.Dinter, and K.Tesch. Longitudinal attenuation of dose equivalent in a concrete shield for high energy proton beams. Internal Report DESY D3-85, 1996.

[3] I.L.Azhgirey, I.A.Kurochkin, A.V.Sannikov, and E.N.Savitskaya. *Nucl.Instr.Meth.*, A408:535, 1998.

[4] C.Birattari, E.DePonti, A.Esposito, A.Ferrari, M.Magugliani, M.Pelliccioni, T.Rancati, and M.Silari. Measurements and simulations in high energy neutron fields. In *SATIF-2*. CERN-OECD-NEA, 1995.

[5] D.Dworak, K.Tesch, and J.M.Zazula. *Nucl.Instr.Meth*, A321:589, 1992.

[6] Y.Nakane, Y.Sakamoto, K.Hayashi, and T.Nakamura. Intercomparison of neutron transmission benchmark analysis for iron and concrete shields in low, intermediate and high energy proton accelerator facilities. In *SATIF-3*, Tokyo University Sendai, 1997. OECD-NEA.

[7] H.Hirayama. Intercomparison of the medium-energy neutron attenuation in iron and concrete. In *SATIF-3*, Tokyo University Sendai, 1997. OECD-NEA.

[8] H.Dinter, J.Pang, and K.Tesch. *Rad. Protection Dosimetry*, 25:107, 1988.

[9] H.Dinter, J.Pang, and K.Tesch. *Rad. Protection Dosimetry*, 28:207, 1989.

[10] A.Fasso, A.Ferrari, and P.R.Sala. Designing electron accelerator shielding with FLUKA. In *8th Intern. Conf. Radiation Shielding*, Arlington, 1994.

[11] X.Mao, K.R.Kase, and W.R.Nelson. *Health Physics*, 70:207, 1996.

[12] D.Dworak, J.Łoskiewicz, H.Dinter, A.Leuschner, and K.Tesch. The Monte Carlo calculated spectra and angular distributions of secondary particles from 3, 30, 250 GeV electron interactions in thick Al, Cu, Nb, and Pb targets. Report no. 1840/AP, Institute of Nuclear Physics, Kraków, January 2000.

[13] Landolt-Börnstein. *Numerical data in science and technology*, volume 11: Shielding against high energy radiation. Springer Verlag, 1990.

[14] W.P.Swanson. Radiological safety aspects of the operation of electron linear accelerators. Technical Report Series 188, IAEA, Vienna, 1979.

[15] G.Bathow, E.Freytag, and K.Tesch. *Nucl. Phys.*, B2:669, 1967.

[16] P.Degtyarenko and G.Stapleton. Parametrization for shielding electron accelerators based on Monte Carlo studies. In *Conf. Health Physics of Radiation-Generating Machines*, San Jose, 1997. Health Physics Society.

[17] W.P.Swanson. *Health Physics*, 37:347, 1979.

[18] K.Tesch. *Particle Accelerators*, 9:201, 1979.

[19] K.Tesch. *Rad. Protection Dosimetry*, 22:27, 1988.

[20] A.Fasso, M.Höfert, and A.Ioannidou. *Rad. Protection Dosimetry*, 38:301, 1991.

[21] G.Baur and A.Leuschner. *Eur. Phys. J.*, C8:631, 1999.

Figures

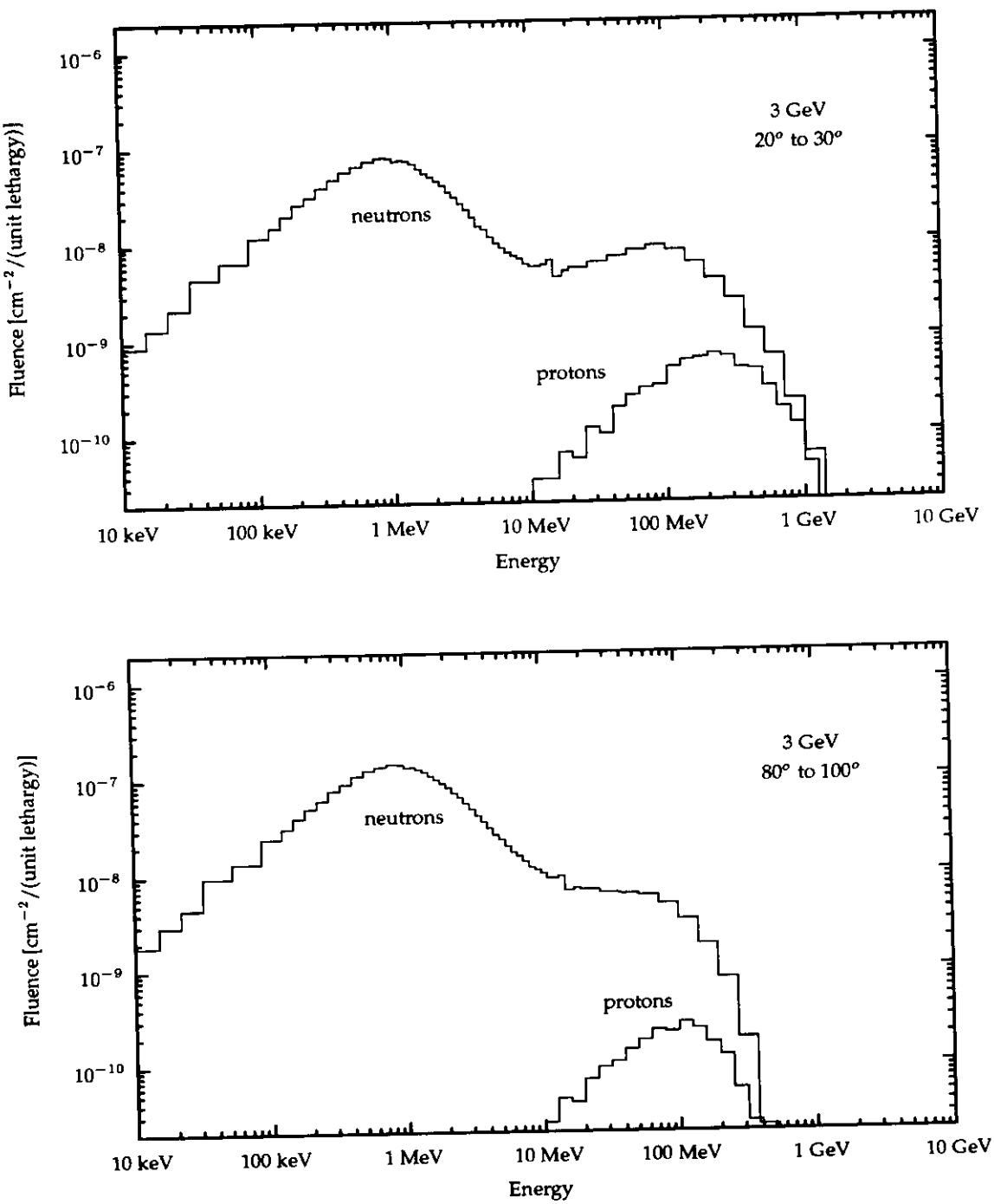

Figure 1: Fluences of neutrons and protons per logarithmic energy interval per one 3-GeV electron, Cu target, distance 500 cm. Upper part: angular interval 20^{O} to 30^{O}. Lower part: angular interval 80^{O} to 100^{O}.

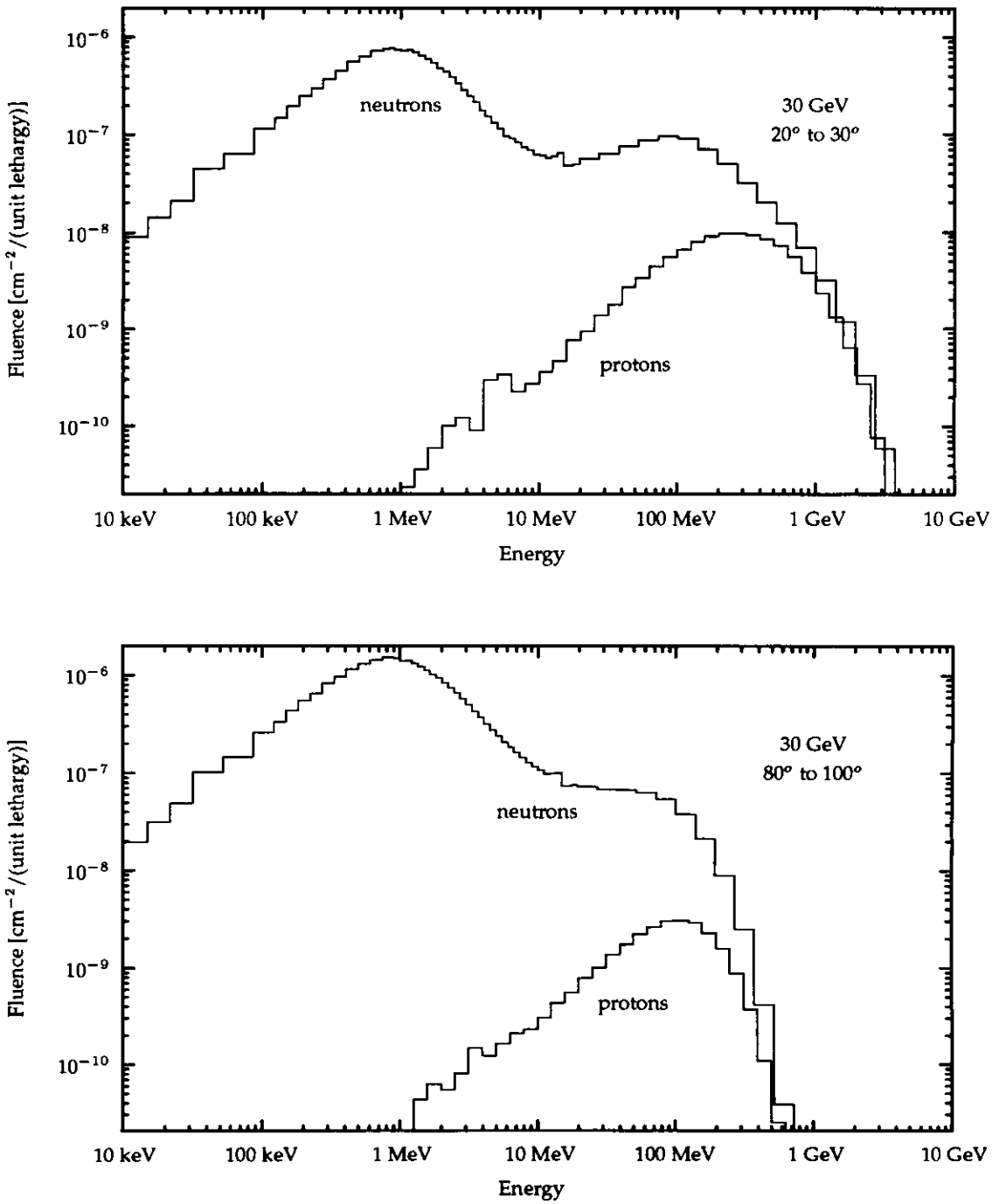

Figure 2: Fluences of neutrons and protons per logarithmic energy interval per one 30-GeV electron, Cu target, distance 500 cm. Upper part: angular interval 20^{O} to 30^{O}. Lower part: angular interval 80^{O} to 100^{O}.

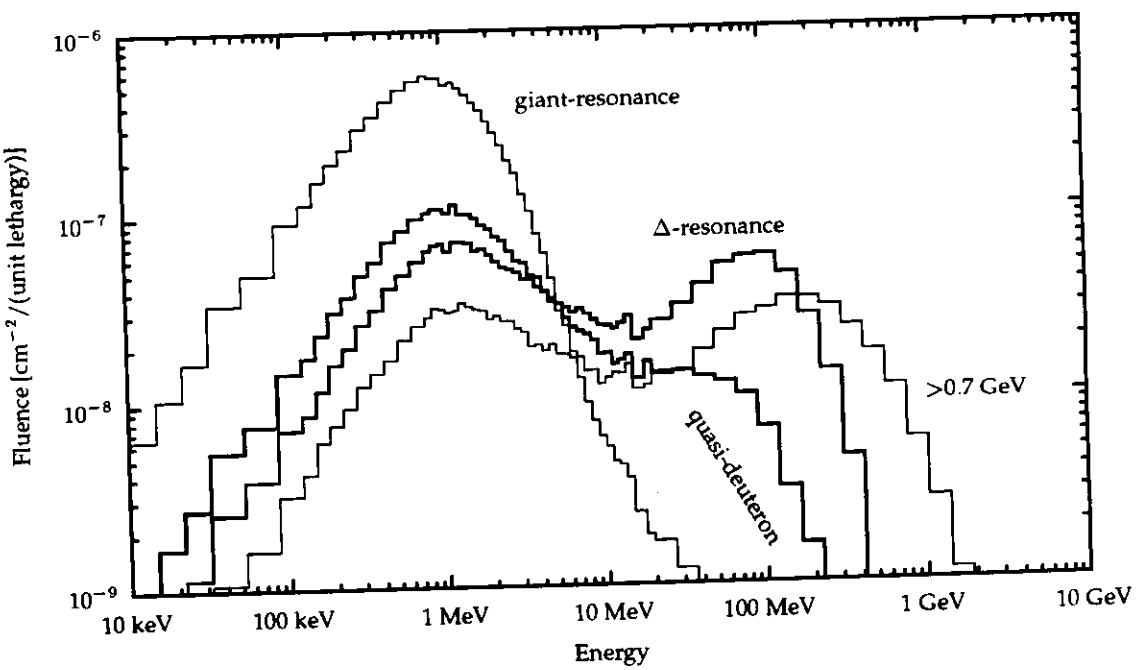

Figure 3: Neutron fluence spectra produced by 4 mechanisms: giant-resonance interaction, quasi-deuteron disintegration, Δ-resonance production, interactions with $E_\gamma > 0.7$ GeV. Fluence is given per logarithmic energy interval per one 30-GeV electron, Cu target, angular interval 20^o to 30^o, distance $r = 500$ cm.

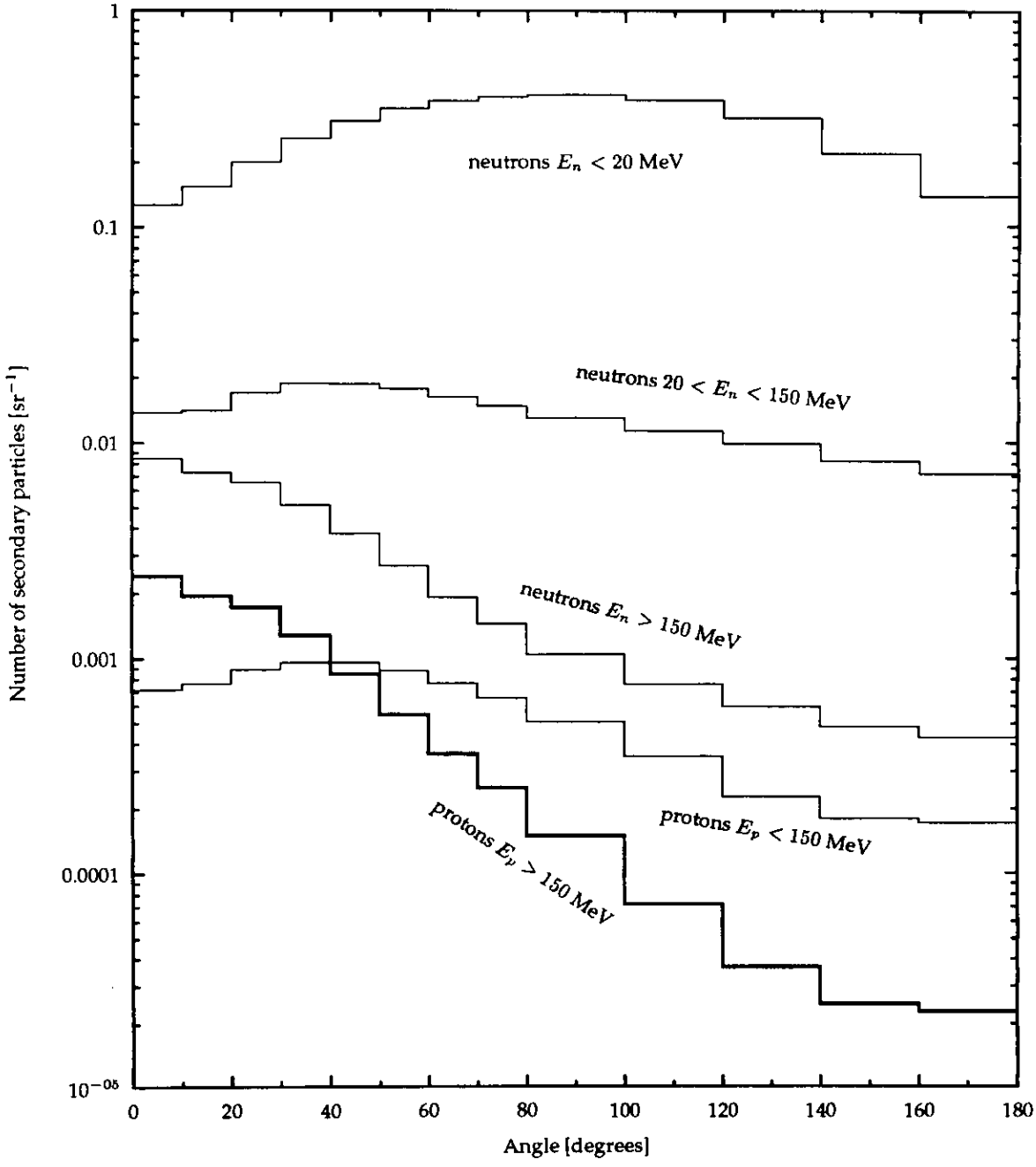

Figure 4: Angular distributions of neutrons and protons around the copper target for one 30-GeV electron.

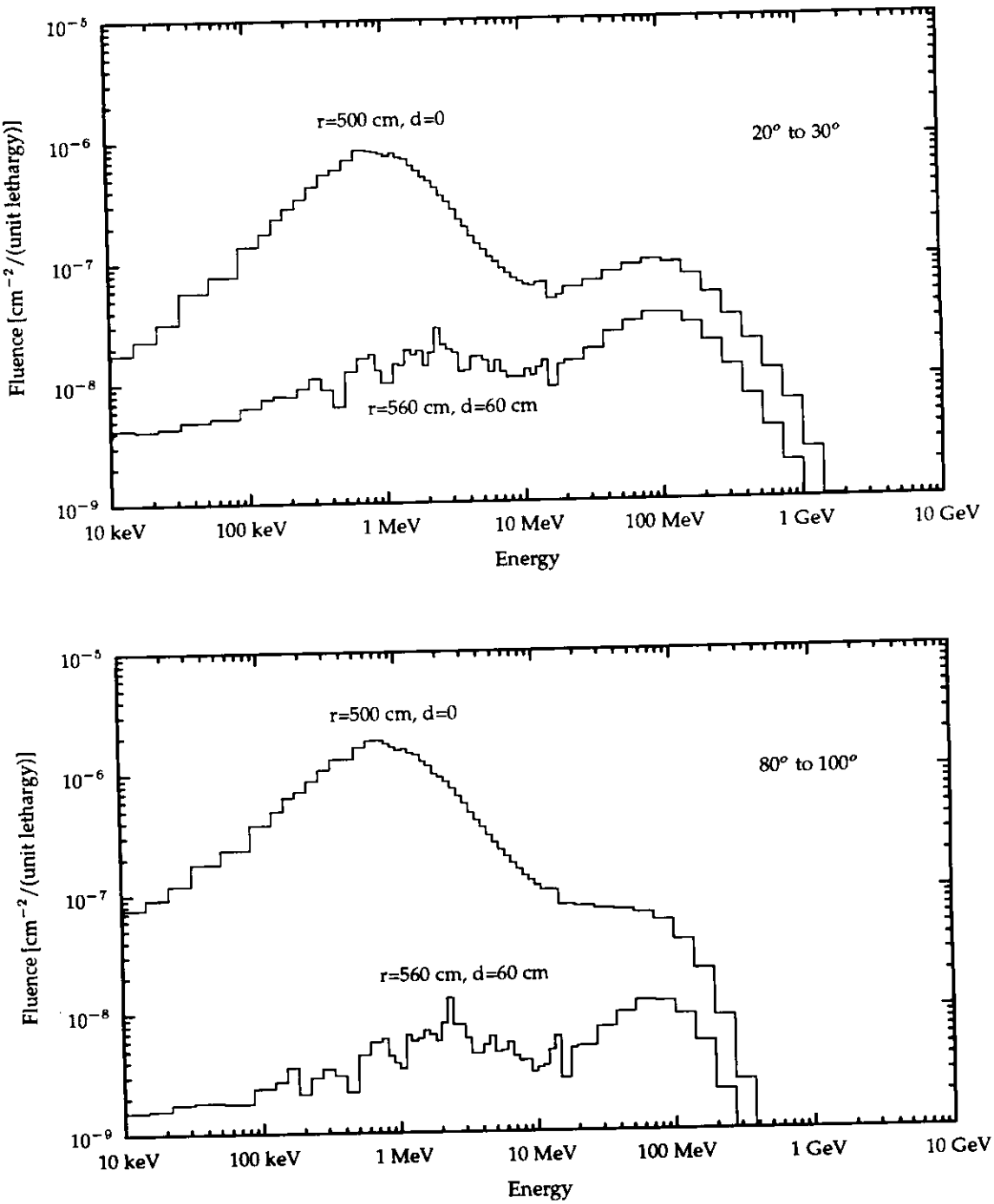

Figure 5: Neutron fluence spectra behind 60 cm concrete compared with the source spectra. Fluences are given per logarithmic energy interval per one 30-GeV electron, Cu target, distances r = 500 cm, concrete thickness d = 0 (source) and r = 560 cm, d=60 cm. Upper part: angular interval 20^{O} to 30^{O}. Lower part: angular interval 80^{O} to 100^{O}.

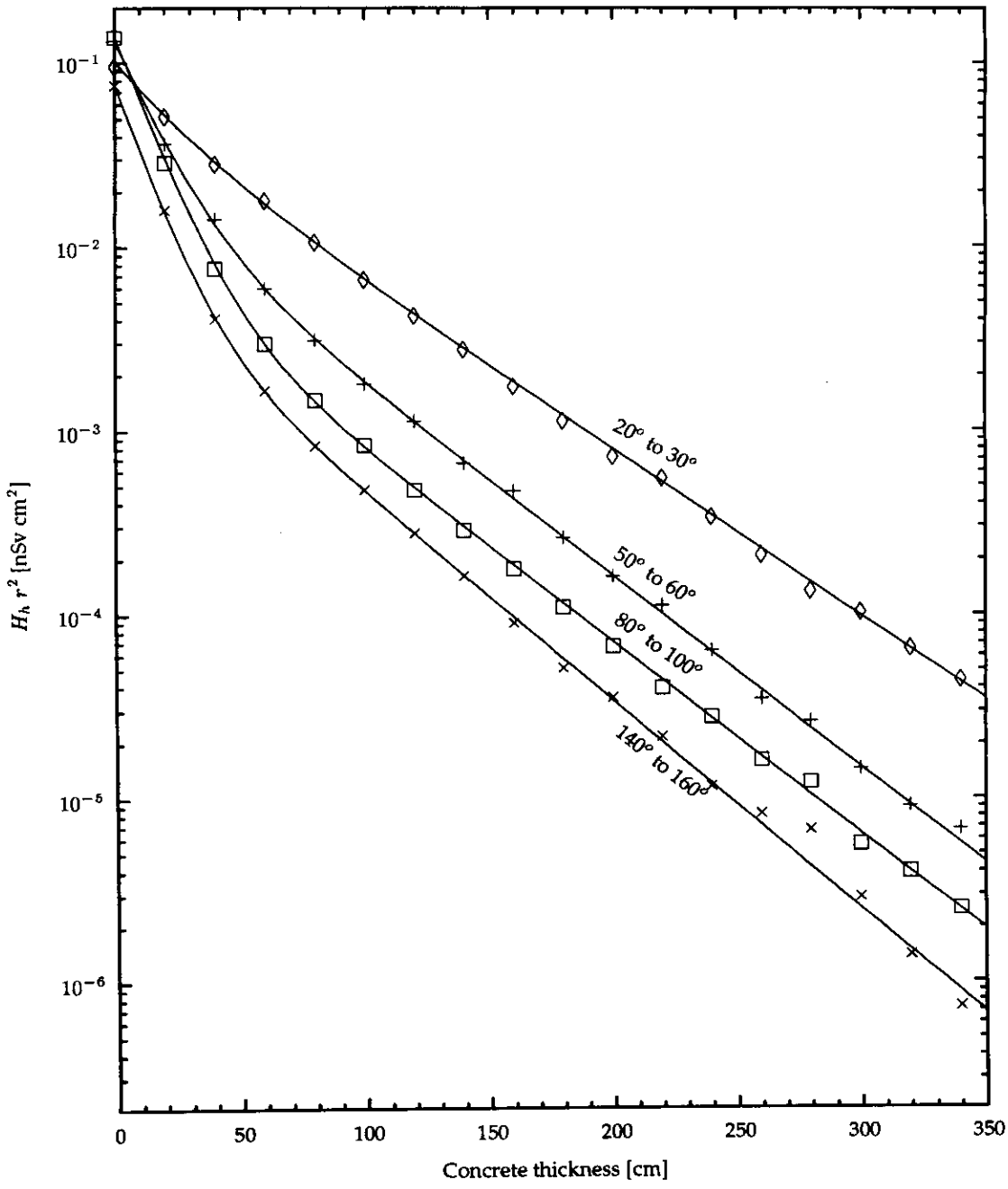

Figure 6: Attenuation of the total hadron dose equivalent in concrete at 4 angular intervals produced by one 30-GeV electron in the Cu target. The dose is multiplied by the squared distance from the target.

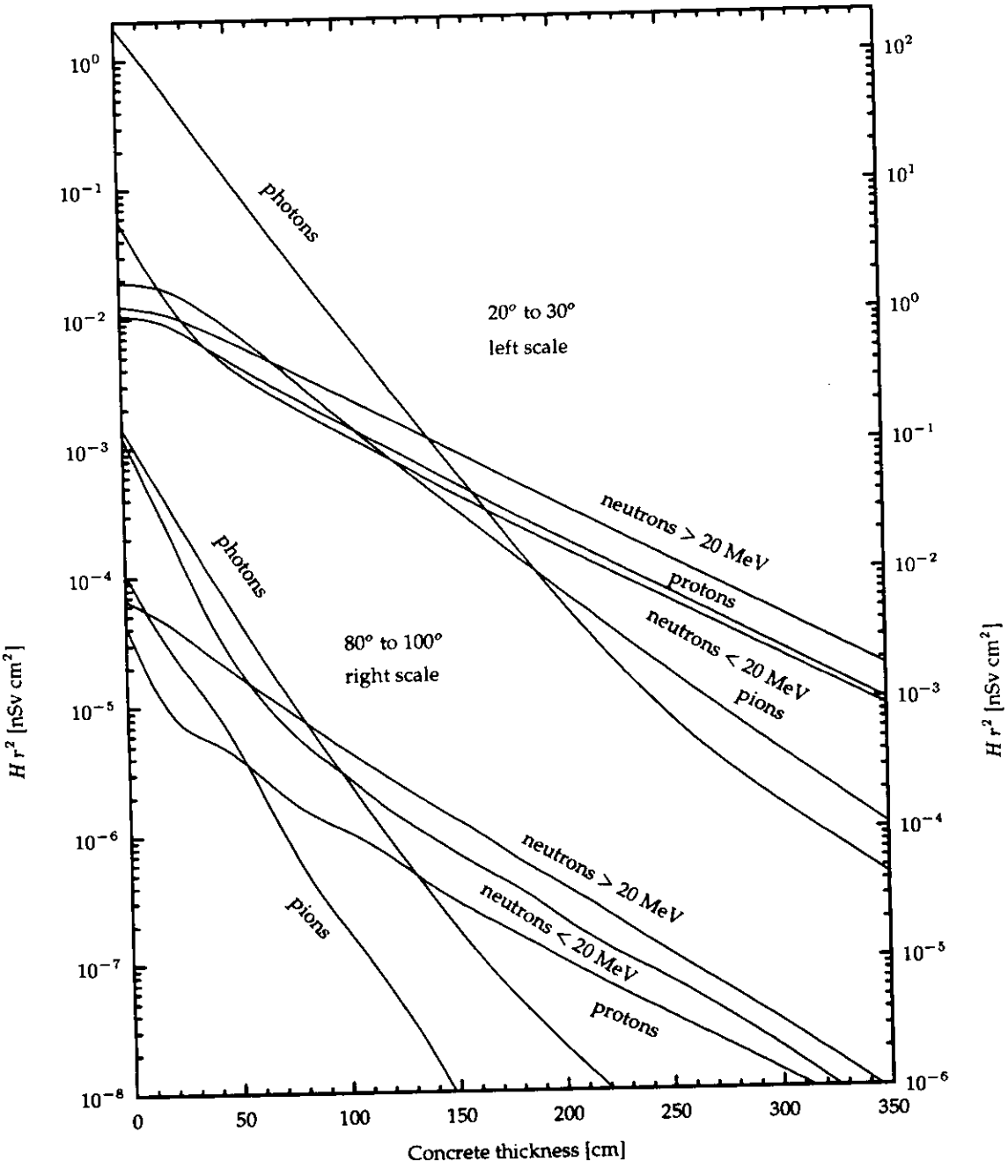

Figure 7: Attenuation of 4 hadron dose equivalent components in concrete at 2 angular intervals. The dose is multiplied by the squared distance from the target, E_o = 30 GeV, Cu target. The electron-photon dose is added.

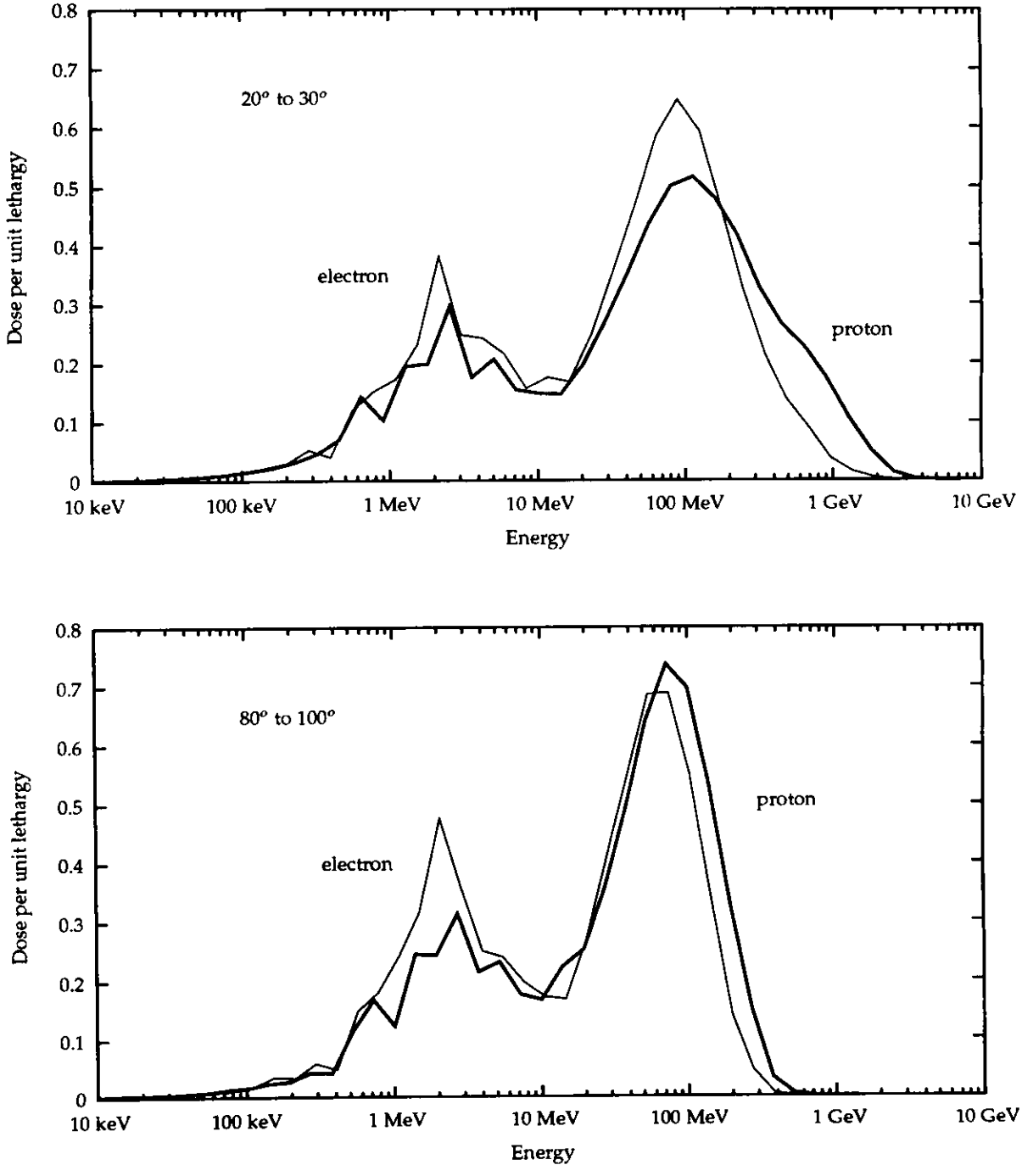

Figure 8: Neutron dose spectra behind 60 cm concrete produced by 30-GeV electrons (thin line) and 30-GeV protons (thick line). Doses are given per logarithmic energy interval normalized to unity, Cu target. Upper part: angular interval 20^{o} to 30^{o}. Lower part: angular interval 80^{o} to 100^{o}.

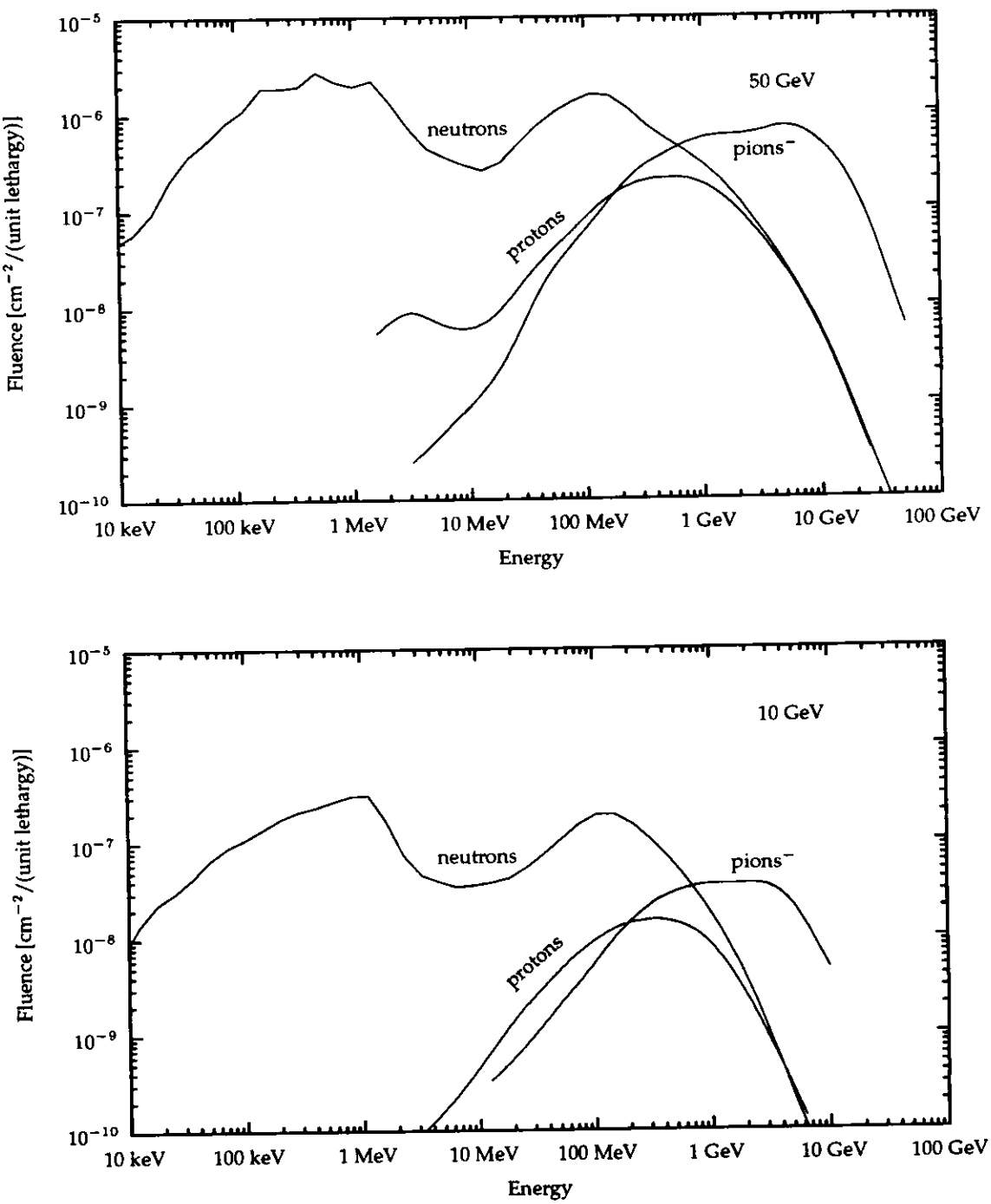

Figure 9: Fluence spectra of neutrons, protons and negative pions per logarithmic energy interval per one primary electron 100 cm behind a 50 cm Cu absorber in beam direction. Upper part: $E_o = 50$ GeV. Lower part: $E_o = 10$ GeV.